# Hyperspectral Blind Reconstruction from Random Spectral Projections

Gabriel Martín and José M. Bioucas-Dias, *Senior Member, IEEE*

***Abstract*—This paper proposes a blind hyperspectral reconstruction technique termed *spectral compressive acquisition* (SpeCA) conceived to spaceborne sensors systems, which are characterized by scarce onboard computing and storage resources and by communication links with reduced bandwidth. SpeCA exploits the fact that hyperspectral vectors often belong to a low dimensional subspace and it is blind in the sense that the subspace is learned from the measured data. SpeCA encoder is computationally very light; it just computes random projections with the acquired spectral vectors. SpeCA decoder solves a form of blind reconstruction from random projections whose complexity, although higher than that of the encoder, is very light in the sense that it requires only modest resources to be implemented in real time. SpeCA coding/decoding scheme achieves perfect reconstruction in noise free hyperspectral images and is very competitive in noisy data. The effectiveness of the proposed methodology is illustrated in both synthetic and real scenarios.**

***Index Terms*—Hyperspectral imaging, blind compressive sensing, random projections, low dimensional subspace, linear spectral unmixing, endmember extraction, abundance estimation, random embeddings.**

## I. Introduction

Due to the extremely large volumes of data collected by imaging spectrometers, hyperspectral data compression has received considerable interest in the recent years. These data are usually acquired by a satellite or an airborne instrument and sent to a ground station on Earth for subsequent processing. Usually the bandwidth connection between the satellite/airborne platform and the ground station is reduced, which limits the amount of data that can be transmitted. As a result, there is a clear need for hyperspectral data compression techniques, either lossless or lossy, that can be applied onboard the imaging instrument [1].

Compared with the conventional compression paradigm, the random projection (RP) techniques [2]–[5], which has links with compressive sensing (CS) framework [6], [7], are an attractive alternative in onboard hyperspectral imaging systems, as the compression is performed while acquiring the data, and the bulk of the processing to recover the original data is carried out on the ground, where the constraints on the computing power and the storing are much lighter than those of the onboard imaging systems. In fact, a number of hyperspectral CS and RP methodologies has recently been introduced [2], [3], [4], [8]–[13].

G. Martín and J. M. Bioucas-Dias are with the Instituto de Telecomunicações, Instituto Superior Técnico, Lisbon, 1049-1, Portugal.

This work was supported by the Portuguese Science and Technology Foundation under Project UID/EEA/50008/2013 and Project SFRH/BPD/94160/2013.

At this point, we remark that SpeCA can not be taken as a conventional compression technique, but rather as a form of dimensionality reduction. In fact, in addition to dimensionality reduction, a true compression process necessarily involves much more processing (e.g., quantization and entropy coding), which altogether often yield a considerable higher performance than the CS/RP based methods [14]. Of course, this improved performance usually comes with a price: the need for considerable computing power and storing onboad.

The reconstruction from RP, as in CS, addresses the problem of recovering signals from a number of linear measurements thereof. The success of CS depends critically on the assumption that the underlying signals are sparse or compressible when represented on a suitable frame; a signal is sparse with respect to a given frame if most representation coefficients are zero, and compressible if coefficients have a fast power-law decay. It happens that hyperspectral images (HSIs) are highly correlated in both the spatial and the spectral domains and thus compressible, for example, with respect wavelet frames. It is therefore possible to recover HSIs from a low number of linear measurements, provided that suitable measurement vectors are used. For example in [10], [13], the use of measurement matrices whose elements are independently drawn at random from Gaussian, Bernoulli or (in general) subgaussian distributions yields CS strategies in which the number of measurements, or samples, does not scale with the number of channels.

### A. Proposed Approach and Contributions

Owing to hardware constraints, the implementation of a given RP measurement strategy, involving, for example, dense matrices, may be unattainable. Herein, we propose a measurement strategy operating on the spectral domain, with strong connections with the random embeddings [15]; it computes inner products between the measurement vectors, independently drawn at random from Gaussian, Rademacher, or Bernoulli distributions, and the data spectral vectors. This measurement strategy is light from the hardware point of view and, nevertheless, allows exact recovery from a number of measurements per pixel slightly above the dimension of the subspace and, therefore, does scale with the number of bands. In addition, the complexity of the optimization problem designed to recover the original data is very light.

A fundamental assumption of our approach is that the spectral vectors live in a low dimensional subspace. This a very good approximation in most hyperspectral images (HSIs) of the real world [16], namely when the observed spectral vectors are well approximated by linear mixing model (LMM). In this case, the proposed method performs spectral unmixing while

reconstructing the original data from the random projections; the basis vectors of the subspace are the endmembers and the basis coefficient are the material abundances.

### B. Related Work

The assumption that the hyperspectral vectors live in low dimensional subspace has been recently exploited in a number of works [4], [9]–[13], [17], [18]. The works [9], [10], [13] are nonblind in that they assume that the subspace is known before hand, which is a considerable disadvantage compared with SpeCA, as the later learns the subspace from the random projections. A Compressive-Projection Principal Component Analysis (CPPCA) scheme is introduced in [3] and further developed in [4], [12], [19]. CPPCA is supported in the Rayleigh-Ritz theory to estimate the main principal components and their coefficients from the random projections. One limitation of CPPCA is linked with the fact that the Rayleigh-Ritz method requires well separated eigenvalues, which in HSI images is often true for the first few largest eigenvalues, but usually not true for the smaller eigenvalues, owing to the high degree of correlation among the spectral vectors. In [2] the authors propose a PCA-driven reconstruction which exploit the fact that, under certain conditions, normal Principal Component Analysis (PCA) on low-dimensional random projections of data returns the same result as PCA on the original data set would. The work [11] exploits the randomized singular value decomposition (rSVD) method for the purpose of lossless HSI compression. The core of rSVD is the computation onboard of an orthogonal matrix spanning the data subspace. Compared with SpeCA, this is a disadvantage as the latter does not need to compute such matrix onboard.

### C. Paper Organization

The remainder of the paper is organized as follows. Section II describes SpeCA, a new RP methodology. Section III presents a series of experiments with simulated and real data intended to show the effectiveness of SpeCA. Finally, section IV concludes the paper with some remarks and hints at plausible future research lines.

## II. Problem formulation and proposed solution

In this section, we introduce the SpecCA measurement strategy and the reconstruction algorithm. Let $\mathbf{X} := [\mathbf{x}_1, \dots \mathbf{x}_n] \in \mathbb{R}^{n_b \times n}$ denote a HSI with $n$ spectral vectors (the columns of $\mathbf{X}$) of size $n_b$ (the number of bands of the sensor). We assume that the spectral vectors $\mathbf{x}_i$, for $i = 1, \dots, n$, live in a $p-$dimensional subspace $\mathcal{S}$. This a very good approximation in most real HSIs [16]. Let $\mathbf{M} := [\mathbf{m}_1, \dots, \mathbf{m}_p]$ be a matrix holding a basis for the subspace $\mathcal{S}$ on its columns. Therefore, we may write

$$\mathbf{x}_i = \mathbf{M}\mathbf{s}_i, \quad i = 1, \dots, n, \quad \text{and} \quad \mathbf{X} = \mathbf{M}\mathbf{S},$$

where $\mathbf{s}_i \in \mathbb{R}^p$ is the representation coefficients of $\mathbf{x}_i$ with respect to $\mathbf{M}$, and $\mathbf{S} := [\mathbf{s}_1, \dots \mathbf{s}_n]$. We remark that if the LMM is applicable, $\mathbf{M}$ may be interpretable as the mixing matrix, holding the spectral signatures of the endmembers, and $\mathbf{s}_i$ as the abundance vector of the spectral vector $\mathbf{x}_i$ [16].

### A. The Measurement Strategy

Let's define the measurement matrices $\mathbf{A} \in \mathbb{R}^{m_a \times n_b}$ and $\mathbf{B}_k \in \mathbb{R}^{m_b \times n_b}$ whose elements are independently drawn at random from Gaussian, Rademacher, or Bernoulli distributions. Matrix $\mathbf{A}$ acts on the HSI spectral domain generating $m_a$ measurements per pixel. The measurements obtained with matrix $\mathbf{A}$ are $\mathbf{Y}_a = \mathbf{A}\mathbf{X}$. The measurements obtained with the matrices $\mathbf{B}_k$ are $\mathbf{Y}_b = [\mathbf{y}_{b,1}, \dots, \mathbf{y}_{b,n_v}] \in \mathbb{R}^{m_b \times n_v}$, where $\mathbf{y}_{b,k} = \mathbf{B}_k \mathbf{x}_{i_k} \in \mathbb{R}^{m_b}$, for $k = 1, \dots, n_v$. Matrices $\mathbf{B}_k$ act on pixels with indexes $i_1, i_2, \dots, i_{n_v}$ randomly chosen from the set $1, \dots, n$, producing $m_b$ measurements per sample pixel. Therefore, the total number of measurements per block of $n$ pixels is $m_a n + m_b n_v$ yielding a measurement rate per pixel of $m_a + m_b n_v / n$. We will see in section II-D that for $n \gg n_b p$, and in the absence of noise, perfect reconstruction is possible with $m_b n_v / n \ll 1$.

In the following subsection, we provide two strategies to implement the SpeCA acquisition onto a pushbroom hyperspectral system.

### B. SpeCA Hardware Acquisition Solution

A variety of different hardware designs have been proposed for CS applications [20], [21]. For example, the works [22] and [23] propose a measurement strategy on the spatial domain by using a Digital Micromirror Device (DMD) array. The work [24] proposes a CS system for diffuse optical tomography. Further solutions can be found in [25]–[27].

In this work, we provide two hardware solutions to implement the SpeCA projections. The first solution is based on the work [27] and it schematized in Fig. 1. The measurement system is implemented directly on the instrument optics; therefore, it circumvents the need to acquire the data in full length spectral resolution. The optic system consists mainly of three elements: the first one splits the light into different wavelengths, the second element is a DMD which is programmed to perform multiplication between the signal and random elements; finally, the cylindrical lens sum the reflected light from the DMD producing the final randomly projected observations. The measurements corresponding to matrix $\mathbf{A}$ are obtained by programming the DMD with the same random values for all the pixels at each wavelength, while the measurements corresponding to matrices $\mathbf{B}_k$ are obtained by programming the DMD with different values for each pixel at each wavelength.

A disadvantage of the solution just described is that it requires specific hardware in the hyperspectral sensor; thus, it would not be possible to implement it in an already launched sensor if it does not have this specific hardware. To cope with these limitations, we propose an alternative strategy which consist in implementing the measurement process in electronic hardware.

Fig. 2 schematizes the proposed alternative acquisition strategy operating on a pushbroom hyperspectral acquisition system using the electronic hardware of the sensor. The sensor acquires a complete strip along the cross range direction at once shot; the spectral vectors acquired along the strip are left multiplied by $\mathbf{A}$ and a subset of them are left multiplied by

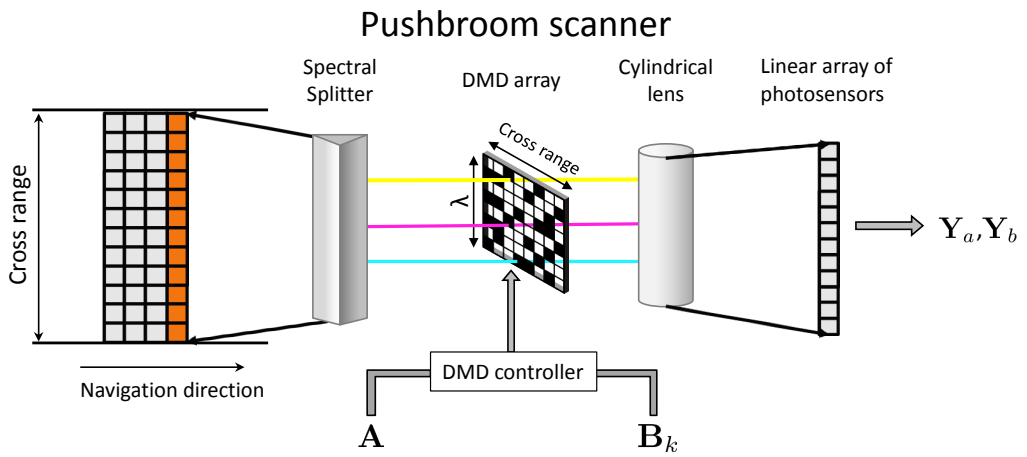


Fig. 1. Scheme of a possible measurement device implemented on a pushbroom satellite sensor using an optic system.

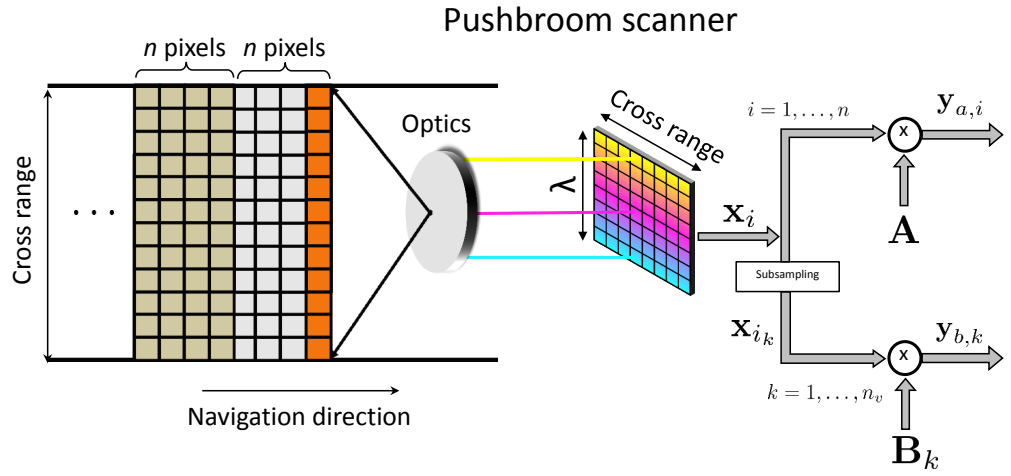


Fig. 2. Scheme of a possible measurement strategy implemented on a pushbroom satellite sensor, using the electronic hardware.

$\mathbf{B}_k$. The sequence $i_1, i_k \ldots, i_{n_v}$ is repeated every block of $n$ pixels.

Although this strategy requires to acquire the data at full spectral resolution, its main advantage, in addition to its simplicity, is that it can be performed line by line and, therefore, only one line need to be saved. In this way, the required storage resources are drastically reduced.

### C. The Reconstruction Algorithm

The proposed recovery algorithm starts by finding a factorization $\mathbf{Y}_a = \mathbf{FS}$, where $\mathbf{F} = \mathbf{AM} \in \mathbb{R}^{m_a \times p}$, $\mathbf{A} \in \mathbb{R}^{m_a \times n_b}$ is the measurement matrix defined above, and $\mathbf{M} \in \mathbb{R}^{n_b \times p}$ holds a basis for the subspace $\mathcal{S}$. Matrix $\mathbf{F}$ may be obtained using, for example, the VCA endmember extraction algorithm [28], parametrized with $p$ endmembers, or the SVD decomposition and retaining the $p$ left singular vectors corresponding to the $p$ larger singular values.

Assuming that $\mathbf{F}$ is full column rank then the solution of $\mathbf{Y}_a = \mathbf{FS}$ with respect to $\mathbf{S}$ is unique and given by $\mathbf{S} = (\mathbf{F}^T\mathbf{F})^{-1}\mathbf{F}^T\mathbf{Y}_a$. Unfortunately, we can not recover $\mathbf{M}$ from the equation $\mathbf{F} = \mathbf{AM}$ because the underlying systems of equations is undetermined. To obtain $\mathbf{M}$, we use the measurements $\mathbf{Y}_b$ jointly with $\mathbf{S}$.

Using the properties of the *vec* and the *kronecker* operators [29], we have

$$\begin{aligned} \mathbf{y}_{b,k} &= \mathbf{B}_k \mathbf{x}_{i_k} && (1)\\ &= \mathbf{B}_k \mathbf{M} \mathbf{s}_{i_k} && (2)\\ &= (\mathbf{s}_{i_k}^T \otimes \mathbf{B}_k)\mathrm{vec}(\mathbf{M}), \quad k = 1 \ldots n_v. && (3) \end{aligned}$$

By stacking all the above equations we obtain the linear system

$$\mathbf{D}\,\mathrm{vec}(\mathbf{M}) = \mathbf{y}_b, \tag{4}$$

with $\mathbf{y}_b = \mathrm{vec}(\mathbf{Y}_b)$, and $\mathbf{D} = [(\widehat{\mathbf{s}}_{i_1} \otimes \mathbf{B}_1^T), \ldots, (\widehat{\mathbf{s}}_{i_{n_v}} \otimes \mathbf{B}_{n_v}^T)]^T$. The solution of (4) is $\mathrm{vec}(\mathbf{M}) = (\mathbf{D}^T\mathbf{D})^{-1}\mathbf{D}^T\mathbf{y}_v$ provided that $\mathbf{D}$ is full column rank, which imply the following conditions:

**i)** $n_v m_b \geq n_b p$, *i.e.* matrix $\mathbf{D}$ must be square or tall

**ii)** the matrix $\mathbf{S}_b \equiv [\mathbf{s}_{i_1}, \mathbf{s}_{i_2} \ldots, \mathbf{s}_{i_{n_v}}]$ must be full row rank; otherwise, the components of the rows of $\mathbf{M}$ orthogonal to span$(\mathbf{S})$ would not be observable

**iii)** the matrix $\mathbf{B} \equiv [\mathbf{B}_{i_1}^T, \mathbf{B}_{i_2}^T \ldots, \mathbf{B}_{i_{n_v}}^T]$ must be full row rank; otherwise, the components of the columns of $\mathbf{M}$ orthogonal to span$(\mathbf{B})$ would not be observable.

The following theorem state sufficient conditions for perfect reconstruction of $\mathbf{X}$ in the absence of noise.

**Theorem 1.** *Assume that the HSI matrix $\mathbf{X} \in \mathbb{R}^{n_b \times n}$ has rank $p \leq \min\{n_b, n\}$ and that the measurement matrices $\mathbf{A} \in \mathbb{R}^{m_a \times n_b}$ and $\mathbf{B}_k \in \mathbb{R}^{m_b \times n_b}$, $k = 1, \ldots, n_v$, with $m_a \geq p$ and $m_b n_v \geq n_b p$, are independently drawn at random from Gaussian $\mathcal{N}(0,1)$, or Rademacher$(1/2)$, or Bernoulli$(1/2)$ distributions. Let $\mathbf{Y}_a = \mathbf{FS} \in \mathbb{R}^{m_a \times n}$ be a factorization of $\mathbf{Y}_a$, where $\mathbf{F} \in \mathbb{R}^{m_a \times p}$ and $\mathbf{S} \in \mathbb{R}^{p \times n}$. Define $\mathbf{S}_b \equiv [\mathbf{s}_{i_1}, \mathbf{s}_{i_2} \ldots, \mathbf{s}_{i_{n_v}}]$ such that a subset of the columns of $\mathbf{S}_b$ of size no smaller than $n_b p$ is at general linear position. In these conditions, $\mathbf{X}$ is exactly recovered from the compressed measurements $\mathbf{Y}_a$ and $\mathbf{Y}_b$ by computing $\mathbf{X} = \mathbf{MS}$, where $\mathbf{M}$ is given by the solution of* (4).

*Proof.* See Appendix. □

The *general position* condition stated in the above theorem means that among the column vectors of $\mathbf{S}_b$, there must be a set of size greater or equal than $n_b p$ such that no hyperplane contains more than $p$ vectors. This condition is not easy to check. However, given that we use $n_v \gg n_b p$, that condition is, in practice, systematically satisfied.

To Summarize, SpeCA reconstruction relies on two steps: 1) Computation of the coefficients $\mathbf{S}$ with respect to a basis of the subspace spanned by the measurements $\mathbf{Y}_a$ obtained with the fixed matrix $\mathbf{A}$ acting on every pixel; 2) Estimation of a signal subspace basis from $\mathbf{S}$ and from the measurements $\mathbf{Y}_b$ obtained with the pixel dependent matrices $\mathbf{B}_k$. As stated in Theorem 1, step 1) depends on $m_a \geq p$ measurements per pixel obtained with $\mathbf{A}$, and the step 2) depends on $m_b n_v \geq n_b p$ measurements obtained with the pixel dependent matrices $\mathbf{B}_k$. We remark that whereas matrix $\mathbf{A}$ acts on every pixel, matrices $\mathbf{B}_k$ may act only in a small subset of pixels as long as the number of measurements obtained with it satisfies $m_b n_v \geq n_b p$. It is clear therefore that the role of the two measurement processes is not interchangeable.

Algorithm 1 shows the pseudo code for the proposed method. Lines 2 and 3 implement the measurements and lines 6 to 12 carry out the HSI reconstruction. Symbol $(\cdot)^\dagger$ in line 7 denotes the Moore-Penrose pseudoinverse. Both processes are illustrated in Fig. 3. The Matlab implementation of the SpeCA algorithm is available online [1]

### *D. A brief note about the measurement rate and SpeCA complexity*

As shown in Theorem 1, in order to ensure perfect reconstruction, the measurement rate must fulfill two conditions.

[1]http://www.lx.it.pt/~bioucas/code/Demo_SpeCA.zip

**Algorithm 1:** Spectral Compressive Acquisition (SpeCA)

**Input**: $\mathbf{A} \in \mathbb{R}^{m_a \times n_b}$, $\mathbf{B}_k \in \mathbb{R}^{m_b \times n_b}, k = 1, \ldots, n_v$ ;
// measurement operators
**Input**: $p$; // dimension of the subspace
**Output**: $\widehat{\mathbf{X}}$ , $\widehat{\mathbf{M}}$, $\widehat{\mathbf{S}}$ ; // estimates

1 **begin** *Measurements*
2 $\quad \mathbf{Y}_a := \mathbf{AX}$;
3 $\quad \mathbf{Y}_b := [\mathbf{y}_{b,1}, \ldots, \mathbf{y}_{b,n_v}], \quad \mathbf{y}_{b,k} := \mathbf{B}_k \mathbf{x}_{i_k}, \ k = 1, \ldots, n_v$;
4 **end**
5 **begin** *HSI Reconstruction*
6 $\quad$ *Find a factorization $\mathbf{Y}_a := \mathbf{FS}$, where $\mathbf{F} \in \mathbb{R}^{m_a \times p}$;*
$\quad$ // Use either VCA or SVD to find $\mathbf{F}$
7 $\quad \widehat{\mathbf{S}} := \mathbf{F}^\dagger \mathbf{Y}_a$; // Use $\mathbf{Y}_b$ and $\widehat{\mathbf{S}}$ to estimate $\mathbf{M}$
8 $\quad \mathbf{y}_{b,i} := \mathbf{B}_k \mathbf{x}_{i_k} := \mathbf{B}_k \mathbf{M} \widehat{\mathbf{s}}_{i_k} \Leftrightarrow \mathbf{y}_{b,i} := (\widehat{\mathbf{s}}_{i_k}^T \otimes \mathbf{B}_k) \text{vec}(\mathbf{M})$;
9 $\quad \mathbf{y}_b := \text{vec}(\mathbf{Y}_b), \quad \mathbf{D} := [(\widehat{\mathbf{s}}_{i_1} \otimes \mathbf{B}_1^T), \ldots, (\widehat{\mathbf{s}}_{i_{n_v}} \otimes \mathbf{B}_{n_v}^T)]^T$ ;
10 $\quad \text{vec}(\widehat{\mathbf{M}}) := \text{solution}\{\mathbf{D}\,\text{vec}(\mathbf{M}) = \mathbf{y}_b\}$;
11 $\quad \widehat{\mathbf{M}} := \text{vec}^{-1}(\text{vec}(\widehat{\mathbf{M}}))$ ; // Reconvert to matrix
12 $\quad \widehat{\mathbf{X}} := \widehat{\mathbf{M}}\widehat{\mathbf{S}}$ ;
13 **end**

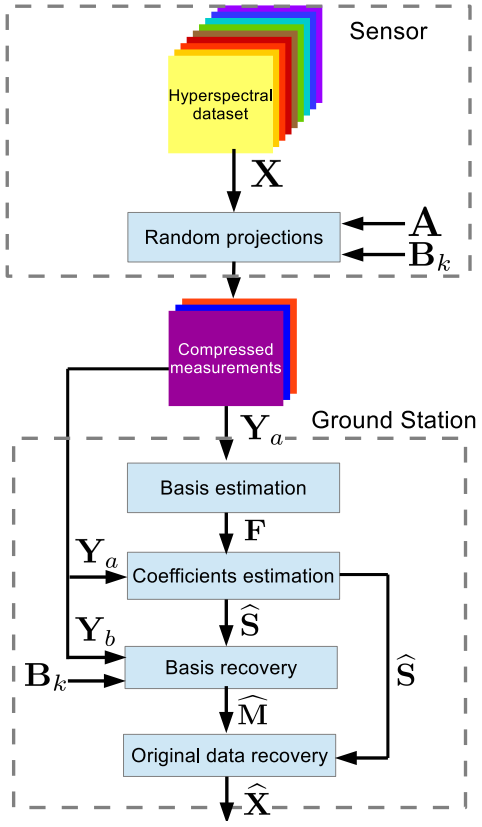


Fig. 3. Flowchart of the compression and the reconstruction process.

The first one is $m_a \geq p$ and is related with the estimation of $\widehat{\mathbf{S}}$. The second one is $n_v m_b \geq n_b p$, which is a necessary condition for matrix $\mathbf{D}$ be full column rank. We conclude therefore that the measurement rate per pixel is $m_a + n_v m_b / n$. In the results shown in the next section, we set $n_v = n$ and $m_b = 1$ yielding a number of measurements per pixel of $m_a + 1$.

Assuming a measurements rate of $m_a + 1$ samples per pixel then the complexity of the associated with the measurements is

of the order of $m_a n_b n$ floating point operations (flops). This complexity is extremely light, in accordance with the main objective of this work. The complexity of the reconstruction algorithm is dominated by the term $p^3 n_b^3$ associated with the solution of the linear system implicit in (4).

### E. Estimation of $p$

The dimension of the subspace $\mathcal{S}$ plays a crucial role in SpeCA. Since we do not know this parameter beforehand, it must be estimated. A simple line of attack consists in setting $m_a$ corresponding to an overestimate of $p$ and then inferring the true vale from $\mathbf{Y}_a$ by exploiting the fact that, in the absence of noise, the rank of that matrix is precisely $p$. Furthermore, as we illustrate in the next section, SpeCA reconstructions are very little sensitive to overestimated values of $p$.

Of course, the proposed scheme to set the value of $p$ is suboptimal and deserves further research, which is, however, out of the scope of this paper.

## III. Results

In this section, we conduct experiments using simulated and real data to illustrate the performance of the proposed approach. As performance indicators, we use the normalized mean squared error (NMSE) between the original image and the reconstructed image (after data compression and decompression) and the peak signal-to-noise ratio (PSNR). The first one is given by

$$\text{NMSE} \equiv ||\widehat{\mathbf{X}} - \mathbf{X}||_F^2 / ||\mathbf{X}||_F^2, \tag{5}$$

and the PSNR is defined as

$$\text{PSNR} \equiv 10 \log_{10} \frac{\max(\mathbf{X})^2 n_b n}{||\widehat{\mathbf{X}} - \mathbf{X}||_F^2}, \tag{6}$$

where $\max(\mathbf{X})$ denotes the maximum over the components of $\mathbf{X}$.

### A. Synthetic data

In our first experiment, we use a synthetic data set generated from spectral signatures randomly selected from the United States Geological Survey (USGS) [2]. The simulated image consists of a set of $5 \times 5$ squares of $10 \times 10$ pixels each one, for a total size of $110 \times 110$ pixels. The first row of squares contains the endmembers, the second row contains mixtures of two endmembers, the third row contains mixtures of three endmembers, and so on. Zero-mean Gaussian noise was added to the synthetic scenes in with signal-to-noise ratios (SNR) defined as $\text{SNR} \equiv 10 \log_{\mathbf{10}} \frac{\|\mathbf{X}\|_F^2}{\mathbb{E}\|\mathbf{N}\|_F^2}$, where $\mathbb{E}$ denotes mean value and $\mathbf{N}$ is the additive noise. Fig. 6 displays the ground-truth abundances maps used for generating the simulated imagery.

The first experiment aims to show the impact of the parameters $m_b$ and $n_v$ on the image reconstruction. In this experiment, we set the parameter $m_a = 5$, the parameter $n_v$ takes values in a range from $0.4n$ to $n$, and the parameter $m_b$ in a range from 1 to 4; thus the averaged number of measurements per pixel $m_b n_v / n$ is between $0.4$ and $4$. Fig. 5 shows the results in terms of PSNR for SNR $\in \{20, 30, 40\}$dB. The plots show that, as expected, increasing the value of the parameters $n_v$ and $m_b$ does not improve significantly the reconstruction accuracy. This is because, as far as the number of measurements $n_v m_b$ satisfies the conditions sated in Theorem 1, the basis of the subspace $\widehat{\mathbf{M}}$ is correctly recovered.

In the remaining experiments we set $m_b = 1$ and $n_v = n$, therefore the measurement rate is then $\delta = (m_a + 1)/n_b$ measurements per pixel per band. We remark that the condition $n_v m_b \geq n_b p$ is satisfied with a large margin.

Table I shows the PSNR for the synthetic image using different values of $m_a \in \{3, 4, 5, 7, 9, 11\}$, for different implementations of SpeCA and without noise. In SpeCA - SVD, the estimation of $\mathbf{F}$ in line 6 in Algorithm 1 has been done taking the first $p$ eigen-vectors of the correlation matrix $\mathbf{Y}_a \mathbf{Y}_a^T$. In SpeCA - VCA the computation of $\mathbf{F}$ has been obtained with the VCA algorithm [28], thus the results can be interpreted as endmembers and abundances fraction maps.

As expected the results show that when the number of measurements $m_a \geq p$ SpeCA yields perfect reconstruction no matter the version of the algorithm used. When $m_a < p$ SpeCA still produces useful reconstructions, although, as expected, the reconstruction error increases as $m_a$ decreases.

Fig. 6 displays PSNR (in dB) values for the synthetic image using different values of $m_a \in \{3, 4, 5, 7, 9, 11\}$ with different noise levels. In this case we use VCA algorithm for the estimation of $\mathbf{F}$. We may conclude that in noisy conditions the accuracy degrades smoothly.

Fig. 7 illustrates SpeCA robustness to $p$. The true value is $p = 5$ and we have run SpeCA with $p \in \{3, 4, \ldots, 10\}$. The figure displays PSNR results provided by SpeCA - SVD algorithm, for different SNR and $m_a = 11$. Clearly, the overestimation of $p$ affects very little the reconstruction accuracy.

### B. Cuprite

In this experiment, we use the well-known AVIRIS Cuprite data set, available online in reflectance units after atmospheric correction. This scene has been widely used to validate the performance of endmember extraction algorithms. The portion used in experiments corresponds to a 240 by 180 pixels subset of the sector labeled as f970619t01p02_r02_sc03a.rfl in the online data. The scene comprises 224 spectral bands between 0.4 and 2.5 $\mu m$, with full width at half maximum of 10 nm and spatial resolution of 20 meters per pixel. Prior to the analysis, several bands were removed due to water absorption and low SNR in those bands, leaving a total of 188 reflectance channels to be used in the experiments.

In this experiment, we evaluate SpeCA robustness with respect to estimation errors in $p$, the dimension of the signal subspace. Having into consideration the estimate $\widehat{p} = 14$ provided by Hysime [30], we input SpeCA with $p = m_a$ taking values between 5 and 19, corresponding to a measurement rate $(m_a + 1)/n_b$ between 0.03 and 0.1. Fig. 8 shows the mean and standard deviation of the PSNR computed from 10 Monte-Carlo runs for SpeCA.

[2] http://speclab.cr.usgs.gov/spectral-lib.html

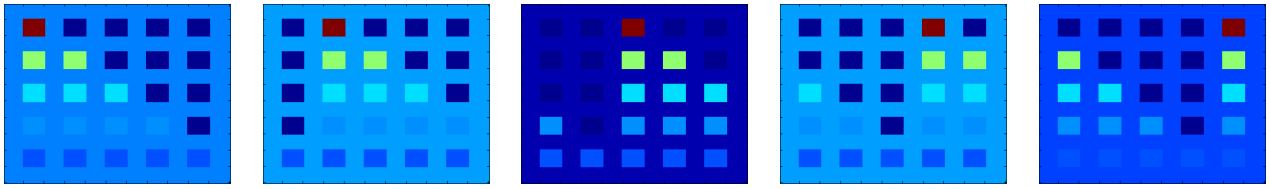

(a) Endmember #1 (b) Endmember #2 (c) Endmember #3 (d) Endmember #4 (e) Endmember #5

Fig. 4. True abundance maps of endmembers in the synthetic hyperspectral data.

TABLE I
SIMULATED DATA. AVERAGE PSNR (IN dB) OBTAINED FROM 10 MONTE-CARLO RUNS FOR DIFFERENT VERSION OF THE METHOD WITHOUT NOISE.

| | $m_a = 3$ | $m_a = 4$ | $m_a = 5$ | $m_a = 7$ | $m_a = 9$ | $m_a = 11$ |
|---|---|---|---|---|---|---|
| SpeCA - SVD | 30.01 | 31.84 | 287.62 | 295.19 | 295.15 | 295.48 |
| SpeCA - VCA | 28.72 | 33.89 | 278.56 | 278.95 | 279.05 | 278.25 |

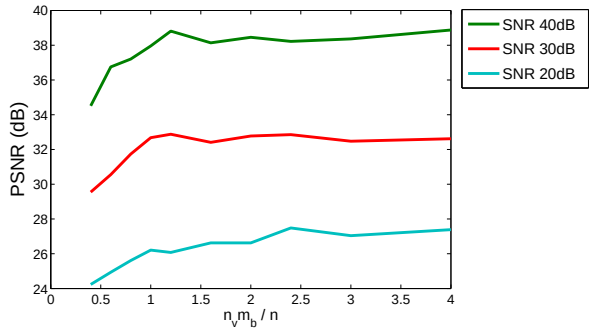


Fig. 5. PSNR (in dB) for the SpeCA method for different values of the parameters $m_b$ and $n_v$ and different SNR when $m_a = 5$, using the synthetic data set.

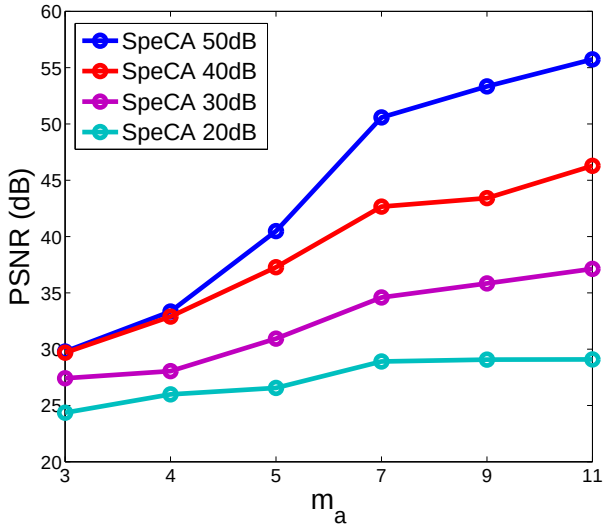


Fig. 6. PSNR (in dB) for the SpeCA method for different samples per pixel $m_a$ and different SNR, using the synthetic data set. Note that the measurement rate is $(m_a + 1)/n_b$.

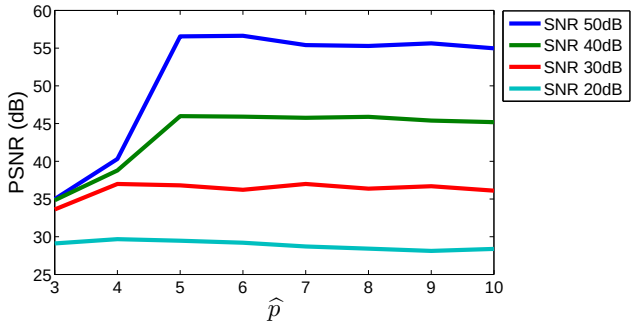


Fig. 7. PSNR between the original and reconstructed image when using different estimations of the size of the subspace $\hat{p}$, in the case of the SpeCA - SVD algorithm for different SNRs and $m_a = 11$.

For comparison purposes, we also show results obtained with state-of-the-art CPPCA [4] and Qi-Hughes methods [2]. The parameters of these methods were hand tuned for optimal performance. In both algorithms, we optimize the number of principal components $L$ to recover. For the different number of measurements $m_a \in \{5, 7, 9, 11, 13, 15, 17, 19\}$, the optimal value of $L$ is, respectively, $\{3, 3, 3, 4, 5, 5, 5, 5\}$ in the case of CPPCA and $\{4, 4, 5, 7, 8, 10, 10, 12\}$ in the case of the Qi-Hughes method. Furthermore, in the case of CPPCA, we optimized the number of partitions of the data set, $J$, in the range $40, \ldots, 2040$ with a step size of 200, resulting in an optimum value of $J = 1640$. From these results, we may conclude that SpeCA produces the best reconstructions, with a very good quality even when $m_a$ is considerable smaller than the true subspace dimension. Qi-Hughes method provide a reconstruction very stable no matter the number of measurements, but worse than SpeCA in all cases. CPPCA lacks stability when the number of measurements is bellow the true signal subspace, but improves its results and stability with a higher number of measurements per pixel.

Fig. 9 shows the NMSE for each pixel in the Cuprite scene using $m_a = 5$ and $m_a = 18$ respectively. When $m_a = 5$ most of the pixels are reconstructed with a very small error (dark blue corresponding to a value around $0.5 \cdot 10^{-3}$)); a very small set of pixels have larger reconstruction errors (red corresponding to a value around $3.5 \cdot 10^{-3}$), as they have part

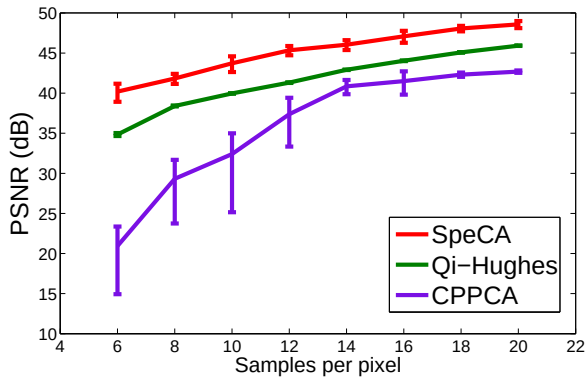


Fig. 8. Mean and variance of the PSNR in the Cuprite data set for SpeCA, CPPCA and Qi-Hughes method for different samples per pixel.

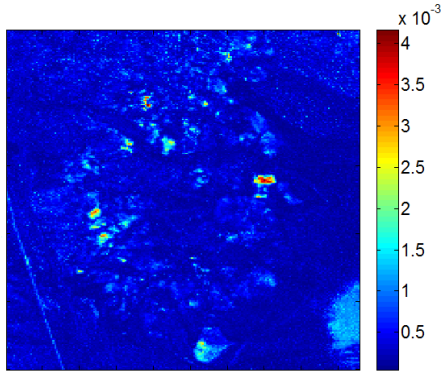

(a) $m_a = 5$

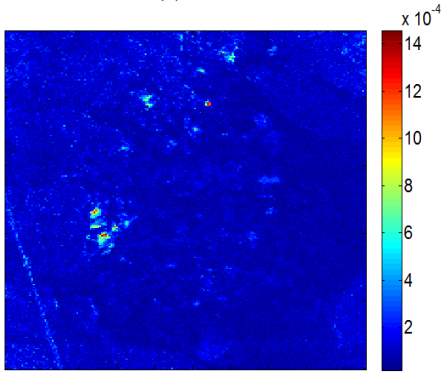

(b) $m_a = 18$

Fig. 9. NMSE for each pixel in the Cuprite dataset when (a) $m_a = 5$ and (b) $m_a = 18$. Note that the measurement rate is $(m_a + 1)/n_b$.

of their energy outside of the range of $\mathbf{Y}_a$. When $m_a = 18$ most of the pixels have a very small error (dark blue $2 \cdot 10^{-4}$) and only few have a larger error of about $12 \cdot 10^{-4}$.

Figs. 10 and 11 show, respectively, a plot of the ordered normalized mean square error per pixel and the reconstructed and the original signatures with highest, mean, and lowest error using different values of $m_a$. We conclude that the large majority of the pixels have a very low reconstruction error, close to a perfect reconstruction. Even in the worst case, the reconstruction obtained with $m_a = 18$ is useful in many applications.

Finally, Fig. 12 shows the results in terms of PSNR with

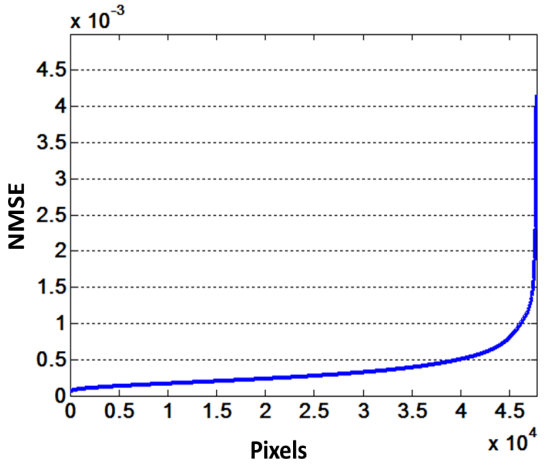


(a) $m_a = 5$

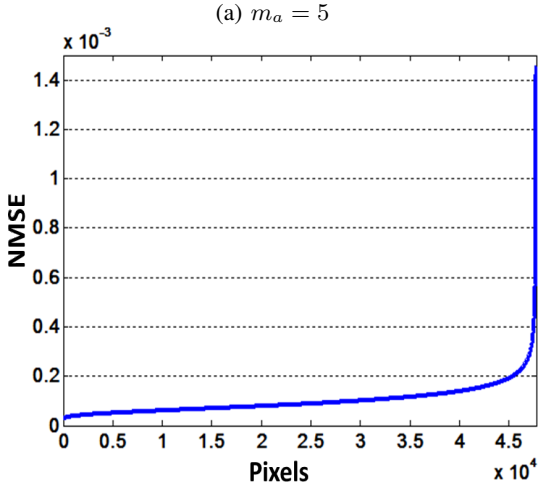


(b) $m_a = 18$

Fig. 10. NMSE per pixel ( $\|\hat{\mathbf{x}}_i - \mathbf{x}_i\|/\|\mathbf{x}_i\|$) for the real Cuprite dataset, using $m_a = 5$ at left and $m_a = 18$ at right. The pixels are ordered from the pixel with lowest error at left to the pixel with highest error at right. Note that the measurement rate is $(m_a + 1)/n_b$.

measurement matrices $\mathbf{A}$ and $\mathbf{B}_k$ sampled from Gaussian, Rademacher, and Bernoulli distributions. The results are similar with a little advantage for the Bernoulli distribution. Thus, we conclude that SpeCA is robust with respect to the statistics used to generate the elements of $\mathbf{A}$ and $\mathbf{B}_k$, at least regarding the three distributions considered.

### C. Pavia University

In this experiment we used the hyperspectral image acquired over the University of Pavia (Italy) by the ROSIS-03 (Reflective Optics Systems Imaging Spectrometer) hyperspectral sensor. The geometrical resolution of the image is 1.3m. In this experiment we used the subset with the first $340 \times 340$ pixels of the Pavia University data set. The original data is composed of 115 spectral bands, ranging from 0.43 to 0.86 $\mu m$ with a band of 4 nm. However, noisy bands were previously discarded, leading to 103 channels.

In this case we input SpeCA with $p = m_a$ in all cases, using different samples per pixel from 6 to 20, thus $m_a$ from 5 to 19, which correspond to a subsample rate from 0.06 to 0.2.

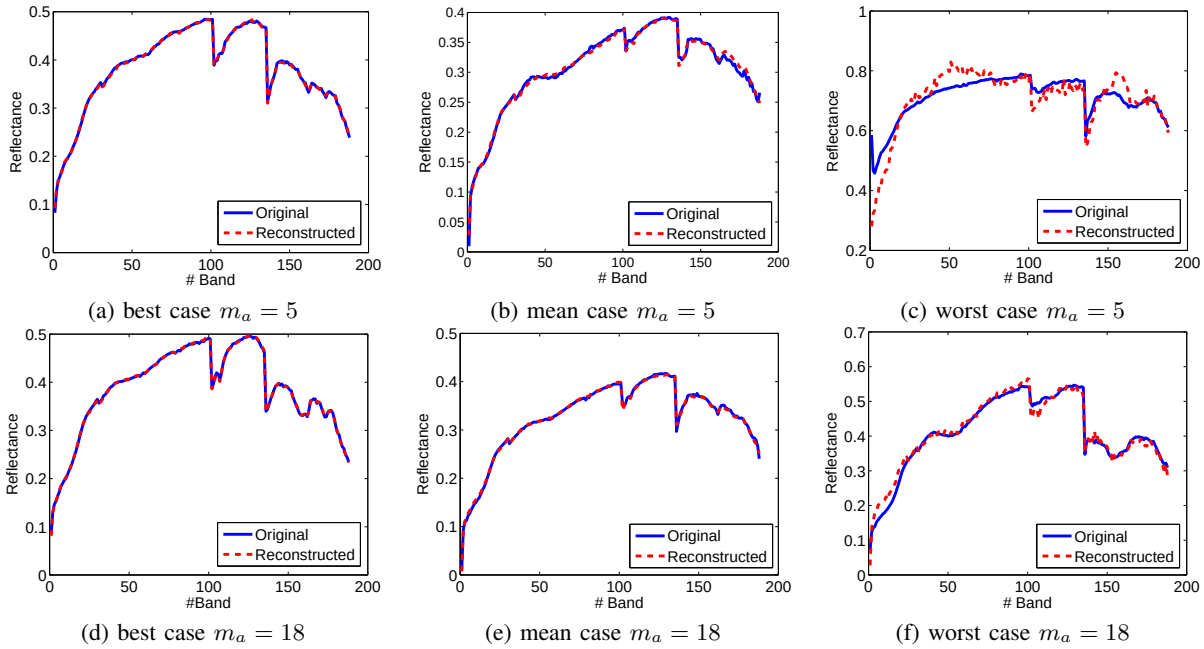


(a) best case $m_a = 5$ (b) mean case $m_a = 5$ (c) worst case $m_a = 5$

(d) best case $m_a = 18$ (e) mean case $m_a = 18$ (f) worst case $m_a = 18$

Fig. 11. Original and reconstructed pixel in the best (a,d), worst(c,f) and mean (b,e) case for the dataset of Cuprite using different values of $m_a$. Note that the measurement rate is $(m_a + 1)/n_b$.

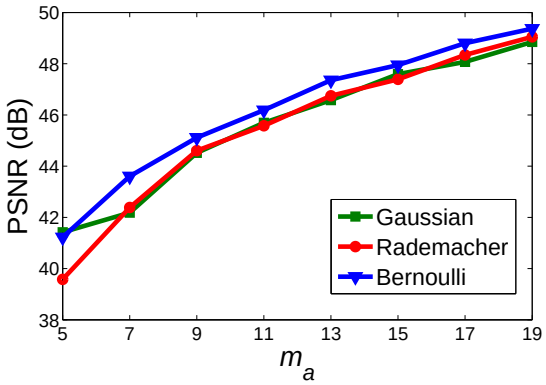


Fig. 12. Mean PSNR after 10 Monte Carlo runs of SpeCA with the Cuprite data set using different types of random matrices for different samples per pixel $m_a$. Note that the measurement rate is $(m_a + 1)/n_b$.

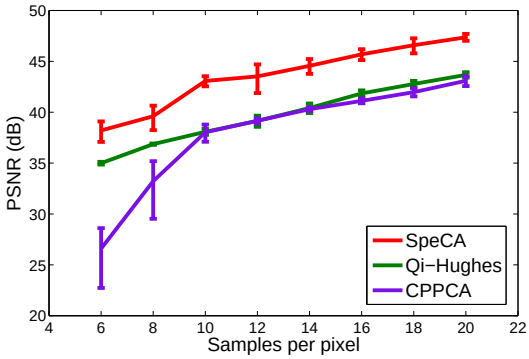


Fig. 13. Mean and variance of the PSNR in the Pavia University data set for SpeCA, CPPCA and Qi-Hughes method for different samples per pixel.

CPPCA and Qi-Hughes paremeters were optimized as in the previous example. Regarding the number of principal components $L$ to recover, and for the different number of measurements $m_a \in \{5, 7, 9, 11, 13, 15, 17, 19\}$, the optimum value was, respectively, $\{2, 3, 4, 5, 5, 6, 7, 8\}$ in the case of CPPCA and $\{3, 3, 4, 6, 8, 10, 11, 11\}$ in the case of Qi-Hughes method. For CPPCA, the number of partitions of the data set, $J$, were optimized in the range $40, \ldots, 2040$ with a step size of 200, resulting in an optimum value of $J = 840$.

Fig. 13 shows the mean PSNR and standard deviation after 10 Monte-Carlo runs for SpeCA, CPPCA and Qi-Hughes methods for the different considered samples per pixel. This experiment shows that SpeCA provides the best results.

### *D. Processing time*

The last experiment aims at showing that SpeCA also is very light from the computational point of view. For this experiment, we used Matlab implementations, that although may not be optimal, give guidelines about the computational complexity. The system used has a quad-core Intel i7- 4790 CPU, 3.6-GHz clock speed and 32-GB RAM. The experiments were run on a Linux Mint 17 OS with the 2013a version of Matlab software.

Table II shows SpeCA, CPPCA and Qi-Hughes execution times for the decoding using different number of measurements per pixel. The parameters used in the case of CPPCA and Qi-Hughes methods were the optimal values described in previous section. SpeCA is the fastest method in all cases and provides an execution time relatively low supporting the claim that SpeCA is a very light from the computational point of view and thus suitable for real-time applications.

TABLE II
EXECUTION TIME IN SECONDS, FOR SPECA, CPPCA AND QI-HUGHES METHOD, USING DIFFERENT MEASUREMENTS PER PIXEL OVER THE CUPRITE DATASET.

| Samples per pixel | 6 | 8 | 10 | 12 | 14 | 16 | 18 | 20 |
|---|---|---|---|---|---|---|---|---|
| SPECA time in secs | 2.44 | 4.32 | 6.48 | 10.36 | 12.67 | 19.67 | 20.60 | 25.09 |
| CPPCA time in secs | 15.30 | 15.58 | 15.94 | 21.38 | 27.05 | 27.60 | 28.14 | 27.24 |
| Qi-Hughes time in secs | 25.09 | 25.98 | 34.01 | 50.23 | 59.87 | 76.11 | 79.97 | 101.91 |

## IV. CONCLUSIONS AND FUTURE RESEARCH LINES

This paper introduced SpeCA, a new method to perform compressive mesurements via random projections over hyperspectral images. SpeCA performs compression in the spectral domain and exploits the low dimensionality of HSIs. SpeCA is blind in the sense that it estimates both the basis of the subspace and the respective coefficients, contrarily to other similar CS techniques, which need to know the basis of the subspace beforehand. SpeCA yields perfect reconstruction in the absence of noise, provided that the number of measurements is larger that a critical limit. When the number of measurements is below the critic limit, SpeCA performance degrades smoothly. SpeCA is very light from the computational point of view, which is a desired feature in real-time applications. In the future, further work will be focused on the implementation of SpeCA using high performance computing architectures such as GPUs in order to perform image reconstruction in real time.

## APPENDIX
## PROOF OF THEOREM 1

*Proof.* Given the measurement matrices $\mathbf{Y}_a = \mathbf{AX} \in \mathbb{R}^{m_a \times n}$ and $\mathbf{Y}_b = [\mathbf{y}_{b,1}, \ldots, \mathbf{y}_{b,n_n}] \in \mathbb{R}^{m_b \times n_v}$, with $\mathbf{y}_{b,k} = \mathbf{B}_k \mathbf{x}_{i_k}$, for $k = 1, \ldots, n_v$, the objective is to prove that the original HSI is given by $\mathbf{X} = \mathbf{MS} \in \mathbb{R}^{n_b \times n}$, where $\mathbf{M} \in \mathbb{R}^{n_b \times p}$ and $\mathbf{S} \in \mathbb{R}^{p \times n}$. Matrix $\mathbf{M}$ is the solution of the linear system $\mathbf{D}\,\mathrm{vec}(\mathbf{M}) = \mathrm{vec}(\mathbf{Y}_b)$, where

$$\mathbf{D} = [(\widehat{\mathbf{s}}_{i_1} \otimes \mathbf{B}_1^T), \ldots, (\widehat{\mathbf{s}}_{i_{n_v}} \otimes \mathbf{B}_{n_v}^T)]^T. \tag{7}$$

Matrix $\mathbf{F}$ results from any factorization $\mathbf{Y}_a = \mathbf{FS}$, with $\mathbf{F} \in \mathbb{R}^{m_a \times p}$.

Given that $\mathbf{A} \in \mathbb{R}^{m_a \times n_b}$ is drawn at random from Gaussian $\mathcal{N}(0,1)$, or Rademacher$(1/2)$, or Bernoulli$(1/2)$ distributions, then the set of rows of $\mathbf{A}$ are in a general linear position with probability one. Since $m_a \leq n_b$, the rows of $\mathbf{A}$ form a linearly independent set and no linear combination falls in the null space of $\mathbf{X}^T$. Since $m_a \geq p$, then $\mathbf{Y}_a$ spans the range of $\mathbf{X}^T$. Therefore, $\mathbf{Y}_a$ has rank $p$ and thus may be factorized as $\mathbf{Y}_a = \mathbf{FS}$, where $\mathbf{F} \in \mathbb{R}^{m_a \times p}$ is full column rank and $\mathbf{S} \in \mathbb{R}^{p \times n}$ is full column rank.

Since $\mathbf{X} \in \mathbb{R}^{n_b \times n}$ has rank $p \leq \min\{n_b, n\}$, we may write $\mathbf{X} = \mathbf{ES}'$, where $\mathbf{E} \in \mathbb{R}^{n_b \times p}$ is any full column rank matrix which spans the range of $\mathbf{X}$ and $\mathbf{S}' \in \mathbb{R}^{p \times n}$ is full row rank. From $\mathbf{AX} = \mathbf{FS}$, we conclude that $\mathbf{AES}' = \mathbf{FS}$ and that $\mathbf{S}' = (\mathbf{AE})^\dagger \mathbf{FS}$, where $(\mathbf{AE})^\dagger$, using the same arguments as above, is full rank. Therefore, we conclude that $\mathbf{X} = \mathbf{MS}$, where $\mathbf{M} = \mathbf{E}(\mathbf{AE})^\dagger \mathbf{F}$.

In order to compute $\mathbf{M}$, we use the set of equations $\mathbf{y}_{b,k} = \mathbf{B}_k \mathbf{M} \mathbf{s}_{i_k}$, for $k = 1, \ldots, n_v$, where we have used the fact $\mathbf{x}_{i_k} = \mathbf{M}\mathbf{s}_{i_k}$. If we apply the operator vec to both sides of $\mathbf{y}_{b,k} = \mathbf{B}_k \mathbf{M} \mathbf{s}_{i_k}$, we obtain the linear system of equations

$$\mathbf{D}\,\mathrm{vec}(\mathbf{M}) = \mathrm{vec}(\mathbf{Y}_b), \tag{8}$$

where $\mathbf{D} \in \mathbb{R}^{(n_v m_a) \times (n_b p)}$ is given by (7). The system (8) has a unique solution if and only if the null space of $\mathbf{D}$ is $\{\mathbf{0}\}$, which implies that $n_v m_a \geq n_b p$ and is equivalent to

$$\{\mathbf{M} : \mathbf{B}_k \mathbf{M} \mathbf{s}_{i_k} = \mathbf{0}, k = 1, \ldots, n_v\} = \emptyset \tag{9}$$

Noting that $\mathbf{B}_k$, for $k = 1, \ldots, n_v$, are drawn at random from Gaussian $\mathcal{N}(0,1)$, or Rademacher$(1/2)$, or Bernoulli$(1/2)$ distributions, that there exist, by hypothesis, a subset of the columns of $\mathbf{S}_b \equiv [\mathbf{s}_{i_1}, \mathbf{s}_{i_2} \ldots, \mathbf{s}_{i_{n_v}}]$ no smaller than $n_b p$ that is at general linear position, and using the same reasoning as above, we conclude that the set (9) is empty. □

## REFERENCES


[1] G. Motta, F. Rizzo, and J. Storer, *Hyperspectral data compression*. Berlin: Springer, 2006.

[2] H. Qi and S. Hughes, "Invariance of principal components under low-dimensional random projection of the data," in *Proc. 2012 19th IEEE Int. Conf. on Image Processing (ICIP)*. IEEE, 2012, pp. 937–940.

[3] J. Fowler, "Compressive-projection principal component analysis," *IEEE Trans. Image Process.*, vol. 18, no. 10, pp. 2230–2242, 2009.

[4] J. Fowler and Q. Du, "Reconstructions from compressive random projections of hyperspectral imagery," in *Optical Remote Sensing*. Berlin: Springer, 2011, pp. 31–48.

[5] J. Fowler, "Decentralized reconstruction from compressive random projections driven by principal components," in *Proc. 2015 23th European Signal Processing Conf. (EUSIPCO)*. IEEE, 2015, pp. 2157–2161.

[6] D. Donoho, "Compressed sensing," *IEEE Trans. Inf. Theory*, vol. 52, no. 4, pp. 1289–1306, 2006.

[7] E. Candès, J. Romberg, and T. Tao, "Robust uncertainty principles: Exact signal reconstruction from highly incomplete frequency information," *Communications on Pure and Applied Mathematics*, vol. 59, no. 8, p. 1207, 2006.

[8] A. Wagadarikar, R. John, R. Willett, and D. Brady, "Single disperser design for coded aperture snapshot spectral imaging," *Applied optics*, vol. 47, no. 10, pp. B44–B51, 2008.

[9] C. Li, T. Sun, K. Kelly, and Y. Zhang, "A compressive sensing and unmixing scheme for hyperspectral data processing," *IEEE Trans. Image Process.*, vol. 21, no. 3, pp. 1200–1210, 2011.

[10] M. Golbabaee, S. Arberet, and P. Vandergheynst, "Compressive source separation: Theory and methods for hyperspectral imaging," *IEEE Trans. Image Process.*, vol. 22, no. 12, pp. 5096–5110, 2013.

[11] J. Zhang, J. Erway, X. Hu, Q. Zhang, and R. Plemmons, "Randomized SVD methods in hyperspectral imaging," *Journal of Electrical and Computer Engineering*, vol. 2012, p. 3, 2012.

[12] C. Chen, W. Li, E. Tramel, and J. Fowler, "Reconstruction of hyperspectral imagery from random projections using multihypothesis prediction," *IEEE Trans. Geosci. Remote Sens.*, vol. 52, no. 1, pp. 365–374, 2014.

[13] G. Martin, J. Bioucas-Dias, and A. Plaza, "Hyca: A new technique for hyperspectral compressive sensing," *IEEE Trans. Geosci. Remote Sens.*, vol. 53, no. 5, pp. 2819–2831, 2014.

[14] V. Goyal, A. Fletcher, and S. Rangan, "Compressive sampling and lossy compression," *IEEE Signal Processing Mag.*, vol. 25, no. 2, pp. 48–56, 2008.

[15] W. Johnson and J. Lindenstrauss, "Extensions of Lipschitz mappings into a Hilbert space," *Contemporary mathematics*, vol. 26, no. 1, p. 189206, 1984.

[16] J. Bioucas-Dias, A. Plaza, N. Dobigeon, M. Parente, Q. Du, P. Gader, and J. Chanussot, "Hyperspectral unmixing overview: Geometrical, statistical and sparse regression-based approaches," *IEEE J. Sel. Topics Appl. Earth Observations Remote Sens.*, vol. 5, no. 2, pp. 354–379, 2012.

[17] A. Rajwade, D. Kittle, T.-H. Tsai, D. Brady, and L. Carin, "Coded hyperspectral imaging and blind compressive sensing," *SIAM Journal on Imaging Sciences*, vol. 6, no. 2, pp. 782–812, 2013.

[18] S. Gleichman and Y. Eldar, "Blind compressed sensing," *IEEE Trans. Inf. Theory*, vol. 57, no. 10, pp. 6958–6975, 2011.

[19] W. Li, S. Prasad, and J. Fowler, "Integration of spectral–spatial information for hyperspectral image reconstruction from compressive random projections," *IEEE Geosci. Remote Sens. Lett.*, vol. 10, no. 6, pp. 1379–1383, 2013.

[20] A. Liutkus, D. Martina, S. Popoff, G. Chardon, O. Katz, G. Lerosey, S. Gigan, L. Daudet, and I. Carron, "Imaging with nature: Compressive imaging using a multiply scattering medium," *Scientific reports*, vol. 4, p. 5552, 2014.

[21] W. Chan, M. Moravec, R. Baraniuk, and D. Mittleman, "Terahertz imaging with compressed sensing and phase retrieval," *Optics letters*, vol. 33, no. 9, pp. 974–976, 2008.

[22] D. Takhar, J. Laska, M. Wakin, M. Duarte, D. Baron, S. Sarvotham, K. Kelly, and R. Baraniuk, "A new compressive imaging camera architecture using optical-domain compression," in *Proc. SPIE, Computational Imaging IV*, vol. 6065, 2006, pp. 606 509–606 509–10.

[23] F. Magalhães, F. Araújo, M. Correia, M. Abolbashari, and F. Farahi, "Active illumination single-pixel camera based on compressive sensing," *Applied optics*, vol. 50, no. 4, pp. 405–414, 2011.

[24] M. Süzen, A. Giannoula, and T. Durduran, "Compressed sensing in diffuse optical tomography," *Optics express*, vol. 18, no. 23, pp. 23 676–23 690, 2010.

[25] M. Dahan, "Compressive fluorescence microscopy for biological and hyperspectral imaging," in *Proc. 2012 Imaging Systems and Applications*, 2012, p. IM4C.5.

[26] Y. Pfeffer and M. Zibulevsky, "A micro-mirror array based system for compressive sensing of hyperspectral data," Technion - Israel Institute of Technology, Computer Science Department, Haifa, 3200003, Israel, Tech. Rep. CS-2010-01, 2010.

[27] J. Fowler, "Compressive pushbroom and whiskbroom sensing for hyperspectral remote-sensing imaging," in *Proc. 2014 IEEE Int. Conf. on Image Processing (ICIP)*. IEEE, 2014, pp. 684–688.

[28] J. Nascimento and J. Bioucas-Dias, "Vertex Component Analysis: A Fast Algorithm to Unmix Hyperspectral Data," *IEEE Trans. Geosci. Remote Sens.*, vol. 43, no. 4, pp. 898–910, 2005.

[29] C. Van-Loan, "The ubiquitous kronecker product," *Journal of computational and applied mathematics*, vol. 123, no. 1, pp. 85–100, 2000.

[30] J. Bioucas-Dias and J. Nascimento, "Hyperspectral subspace identification," *IEEE Trans. Geosci. Remote Sens.*, vol. 46, no. 8, pp. 2435–2445, 2008.


**Gabriel Martín** received the Computer Engineering degree, the M.Sc., and the Ph.D. degrees in Computers and Communications Technologies from the University of Extremadura, Cáceres, Spain, in 2008, 2010, and 2013, respectively. He has obtained several prices for his PhD. dissertation such as the "Best Iberian PhD. Dissertation in Information System and Technolgies" awarded by the Iberian Association for Information Systems and Technologies, and the "Outstanding PhD Dissertation award" by the University of Extremadura.

He was a Predoctoral Research Associate (funded by the Spanish Ministry of Science and Innovation) with the Hyperspectral Computing Laboratory, University of Extremadura, and is now a Postdoctoral Researcher (funded by FCT) with the Instituto de Telecomunicações, Lisbon, Portugal. His research interests include the development of new techniques for unmixing and compressive sensing of hyperspectral data sets, as well as the efficient processing and interpretation of these data in different types of high-performance computing architectures. Dr. Gabriel Martín has authored or co-authored more than 38 scientific publications. Dr. Martín has served as a Reviewer for the IEEE JOURNAL OF SELECTED TOPICS IN APPLIED EARTH OBSERVATIONS AND REMOTE SENSING and the IEEE TRANSACTIONS ON GEOSCIENCE AND REMOTE SENSING

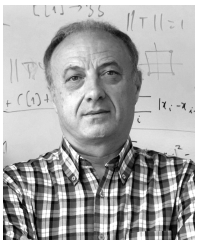

**José M. Bioucas-Dias** (SM'15) received the EE, MSc, PhD, and "Agregado" degrees from Instituto Superior Técnico (IST), Technical University of Lisbon (TULisbon, now University of Lisbon), Portugal, in 1985, 1991, 1995, and 2007, respectively, all in electrical and computer engineering.

Since 1995, José Bioucas-Dias has been with the Department of Electrical and Computer Engineering, IST, where he was an Assistant Professor from 1995 to 2007 and an Associate Professor since 2007. Since 1993, he is also a Senior Researcher with the Pattern and Image Analysis group of the Instituto de Telecomunicações, which is a private non-profit research institution. His research interests include inverse problems, signal and image processing, pattern recognition, optimization, and remote sensing. His research work has been highly cited.

José Bioucas-Dias was an Associate Editor for the IEEE TRANSACTIONS ON CIRCUITS AND SYSTEMS (1997-2000) and IEEE TRANSACTIONS ON IMAGE PROCESSING (2010-2014) and he is a Senior Area Editor for the IEEE TRANSACTIONS ON IMAGE PROCESSING and an Associate Editor for the IEEE TRANSACTIONS ON GEOSCIENCE AND REMOTE SENSING. He was the General Co-Chair of the 3rd IEEE GRSS Workshop on Hyperspectral Image and Signal Processing, Evolution in Remote sensing (WHISPERS'2011) and has been a member of program/technical committees of several international conferences.